Enhanced high-order harmonic generation from periodic potentials in inhomogeneous laser fields

Tao-Yuan Du,[1,2] Zhong Guan,[1,3] Xiao-Xin Zhou,[3] and Xue-Bin Bian[1,*]

[1]*State Key Laboratory of Magnetic Resonance and Atomic and Molecular Physics, Wuhan Institute of Physics and Mathematics, Chinese Academy of Sciences, Wuhan 430071, China*

[2]*University of Chinese Academy of Sciences, Beijing 100049, China*

[3]*College of Physics and Electronic Engineering, Northwest Normal University, Lanzhou 730070, China*

(Received 9 May 2016; published 29 August 2016)

We theoretically study high-order harmonic generation (HHG) from solid-phase systems in spatially inhomogeneous strong laser fields originated by resonant plasmons within a metallic nanostructure. The intensity of the second plateau in HHG may be enhanced by two to three orders and be comparable with the intensity of the first plateau. This is due to bigger transition probabilities to higher conduction bands. It provides us with a practical way to increase the conversion efficiency of HHG with laser intensity below the damage threshold. It presents a promising way to triple the range of HHG spectra in experimental measurements. It also allows us to generate intense isolated attosecond pulses from solids driven by few-cycle laser fields.

DOI: 10.1103/PhysRevA.94.023419

The study of light-matter interaction with intense laser fields is a rapidly growing research area, which exhibits many novel phenomena [1–3]. The high-order harmonic generation (HHG) has attracted a lot of attention since it provides a tabletop coherent x-ray source. It has been used for dynamic imaging of molecular structures [4–6]. However, the low conversion efficiency of HHG from gas-phase systems restricts its applications. Recently, HHG has been experimentally generated from bulk crystals [7–9] and solid rare gases [10]. Due to the high density of solid-state materials, it is possible to generate HHG with higher conversion efficiency and to probe the structure of solids. Vampa *et al.* realized all-optical reconstruction of crystal band structure [11]. This method extends measurement schemes of solid-state material band structures. Theoretically, HHG in solid-state materials involves two contributions (interband and intraband currents). The experimental measurement [7] shows one main plateau in HHG from crystals. However, the theoretical simulations [12,13] reveal double-plateau structures. The primary plateau is a result of the resonant transition between the valence band and the first conduction band, while a weaker second plateau is due to transitions from high-lying conduction bands. The intensity of the second plateau is a few orders lower than that of the first one. This may be the reason why the second plateau has not been well resolved experimentally.

Recently, an alternative technique, named the spatially inhomogeneous field (or source of plasmonic enhancement induced by the bow-tie nanostructure), assisted generation of ultrashort attosecond (1 as $= 10^{-18}$ s) pulses in atoms and molecules, which has attracted much attention both in experiments and theories [14–27]. In comparison with the homogeneous field, the electrons obtain extra energy by further acceleration in the inhomogeneous fields. This alternative technique provides a way to increase the effective intensity of the input laser fields by almost three orders. As we know, the HHG from solids suffers from low damage-threshold intensity. This plasmon-enhanced scheme may overcome this shortage.

In this work, we will theoretically study the HHG from solids in inhomogeneous laser fields induced by the bow-tie structure growing on the semiconductor substrate. To our knowledge, this has not been investigated.

Based on the single-electron approach, we describe the light-solid interaction in one dimension, along the polarization direction of the laser fields. In the length-gauge treatment, the time-dependent Hamiltonian is written as

$$\hat{H}(t) = \hat{H}_0 + exE(x,t), \tag{1}$$

where $\hat{H}_0 = \frac{\hat{p}^2}{2m} + V(x)$ and $V(x)$ is a periodic lattice potential. In our calculations, we choose the Mathieu-type potential [28]. The specific form is $V(x) = -V_0[1 + \cos(2\pi x/a_0)]$, with $V_0 = 0.37$ a.u. and lattice constant $a_0 = 8$ a.u. The band gap and lattice constant mimic the structure of a semiconductor with wide band gap, such as the Zincblende AlN [29–31]. The spatial dependence of the enhanced laser electric field is perturbative and linear with respect to the position, and the laser field can be approximated as (similar to Taylor expansion)

$$E(x,t) \simeq E(t)(1 + \epsilon x), \tag{2}$$

where $\epsilon \ll 1$ is a parameter characterizing the strength of inhomogeneity. The time-dependent Hamiltonian can be rewritten as

$$\hat{H}(t) = \hat{H}_0 + exE(t) + e(\epsilon x^2)E(t), \tag{3}$$

where the first two terms account for the Hamiltonian in the case of homogeneous fields and the last term is an additional term induced by the inhomogeneous field. Since in solids electrons are delocalized through band motion, nondipole corrections [32,33] to radiative interactions should be included. In Fig. 1, we show a schematic illustration of the laser field enhancement using a nanostructure of bow-tie elements. The parameter d and the shape of the nanostructure adjust the field inhomogeneity parameter ϵ.

In the absence of the laser fields, the time-independent Schrödinger equation (TIDSE) can be written as

$$\hat{H}_0\phi_n(x) = E_n\phi_n(x). \tag{4}$$

*xuebin.bian@wipm.ac.cn

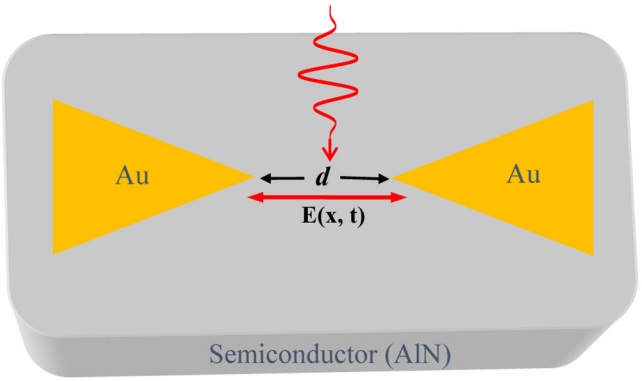

FIG. 1. The nanostructure of bow-tie element. Schematic illustration of laser field enhancement using a nanostructure of bow-tie elements growing on the substrate of semiconductor crystals. The incident direction of the laser pulses is vertical to the substrate.

We use B-spline functions [34] to expand the time-independent wave function,

$$\phi_n(x) = \sum_{i=1}^{N_{\max}} c_i B_i(x). \tag{5}$$

Substituting Eq. (5) into Eq. (4), we obtain matrix equation

$$HC = ESC, \tag{6}$$

where C is the column matrix and H and S are $N \times N$ square matrices, respectively.

We use 2400 B-splines to calculate its eigenvalues in the space region $[-240, 240]$ a.u. and obtain the energy band structure, which agrees well with the calculations by Bloch-state expansion. By using the B-spline basis, we perform all the calculations in the coordinate space. This method is proved to be valid. For the details, we refer readers to Ref. [13]. Due to the drive of laser fields, electrons in the valence band have probabilities to tunnel to conduction bands, i.e., Zener tunneling, but the tunneling probabilities exponentially decay with the increase of energy gap. Only a small portions of populated electrons near the wave vector $k = 0$ on top of the valence band can tunnel to conduction bands with the laser parameters used in the current work. So we choose an initial state calculated by our B-spline method with $k = 0$ on top of the valence band with the minimal band gap. We can effectively solve the time-dependent $|\psi(t)\rangle$ by using symmetric split-operator algorithm [35]

$$|\psi(x,t_0+\Delta t)\rangle = e^{-i\hat{T}\frac{\Delta t}{2}} e^{-i\hat{V}_{\text{eff}}\Delta t} e^{-i\hat{T}\frac{\Delta t}{2}} |\psi(x,t_0)\rangle + O(\Delta t^3), \tag{7}$$

where $\hat{V}_{\text{eff}} = V(x) + ex\,E(x,t)$ and $\hat{T}$ is the kinetic operator.

In our calculations, we use the laser pulses with a $\cos^2$ envelope and the grid spacing is 0.03 a.u., which is sufficient to obtain converged results. The time step is 1/4096 of an optical cycle. In order to prevent spurious reflections from the boundary, the total wave function is multiplied by a mask function of the form $\cos^{1/8}$ with $|x| > 216$ a.u. at each time step. After obtaining the time-dependent $|\psi(t)\rangle$ at an arbitrary time, we can calculate the time-dependent

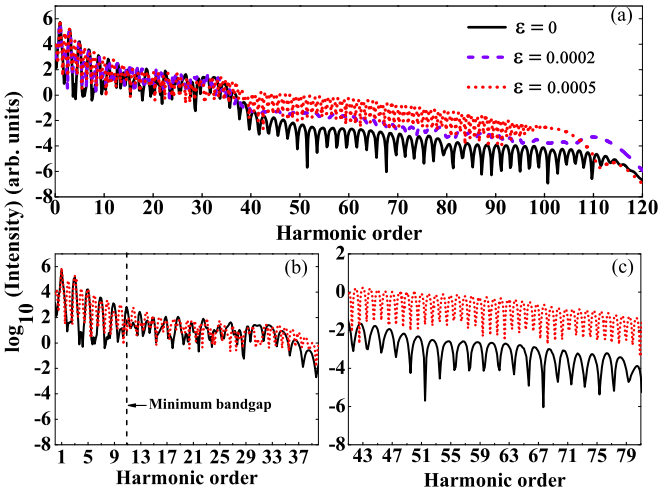

FIG. 2. Comparison of HHG spectra between homogeneous and inhomogeneous fields. HHG spectra in the case of the homogeneous field (black solid curve), the inhomogeneous fields with $\epsilon = 0.0002$ (violet dashed curve), and $\epsilon = 0.0005$ (red dotted curve). (a) HHG with full range. (b) The first HHG plateau with $\epsilon = 0.0005$. (c) The second HHG plateau with $\epsilon = 0.0005$. The intensity, wavelength, and duration of the driving laser pulses are 8.77×10^{11} W/cm^2, 3200 nm, and six optical cycles (o.c.), respectively.

laser-induced currents by

$$j(t) = -\frac{e}{m}[\langle\psi(t)|\hat{p}|\psi(t)\rangle]. \tag{8}$$

The HHG power spectrum is proportional to the modulus square $|j(\omega)|^2$ of Fourier transform of the time-dependent current in Eq. (8). Before the Fourier transform, we multiply $j(t)$ by a time-dependent Hanning window function in order to increase the signal-noise ratio since the intensity of the second plateau is quite low in the homogenous laser field. Based on solid-physics theory, the energy eigenvalues of solid-state materials show a multiple-band structure. Each band group can be distinguished easily as illustrated in Ref. [13]. The intraband contribution to the current is induced by transitions within the same band, while the interband contribution mainly involves transitions between the conduction bands and valence band. By distinguishing the contributions from intra- or interbands, we elucidate the mechanism of intensity enhancement in the second HHG plateau.

First, we study the harmonic spectra of the periodic systems under midinfrared laser pulses. The peak intensity and the wavelength of the driving laser pulses are $I = 8.774 \times 10^{11}$ W/cm^2 and $\lambda = 3200$ nm, respectively. We show the harmonic spectra in the case of the homogeneous and the inhomogeneous fields with different inhomogeneity parameters ϵ in Fig. 2(a). The harmonic spectra show a two-plateau structure in both the homogeneous field and the inhomogeneous field. However, the second HHG plateau exhibits intensity enhancement by two to three orders in the inhomogeneous fields with a small $\epsilon = 0.0005$ compared with the case in the homogeneous field. In order to distinguish the physics behind the harmonic spectra, we show the first HHG plateau in Fig. 2(b) and the second HHG plateau in Fig. 2(c). One can clearly observe both the odd- and

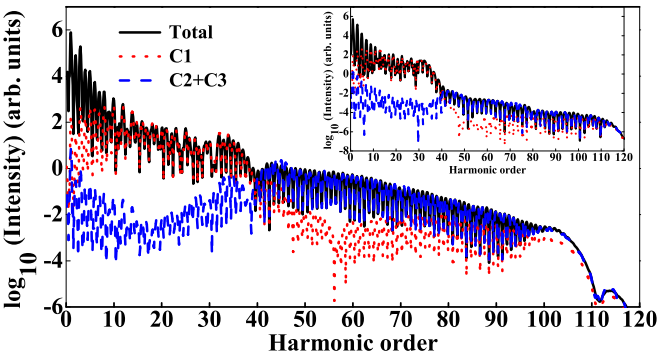

FIG. 3. The distinction of contributions within the conduction bands. HHG induced by full (black solid curve), conduction bands C1 (red dotted curve), and C2 plus C3 (blue dashed curve) contributions in an inhomogeneous field with $\epsilon = 0.0005$. The inset shows the HHG induced by full conduction bands C1 and C2 plus C3 contributions in the homogeneous field. The laser pulse parameters are the same as those in Fig. 2.

even-order harmonics from the HHG spectra in the case of the inhomogeneous field. The generation of the even harmonics is due to the fact that the symmetry of the system is broken. The energy of the first few fast-decaying HHG is lower than the band gap. They show a perturbative character which is similar to the below-threshold HHG in the gas phase [36].

In order to obtain further insights into the effect of spatial inhomogeneity on the HHG process in Fig. 2, we make a distinction about HHG induced by conduction bands C1 and C2 plus C3 contributions in Fig. 3, respectively. The mechanism of the first HHG plateau is mainly determined by interband transitions between the conduction band C1 and the valence band, which have been pointed out by previous researchers in homogeneous fields [11–13]. One can find that the second HHG plateau is the results of interband transitions between conduction bands C2 plus C3 and the valence band. The enhancement of HHG comes from the contribution of these higher conduction bands.

We then perform a time-frequency analysis [37] of the harmonics obtained in Fig. 2, as shown in Figs. 4(a) and 4(b), respectively. However, the harmonic emission behavior changes dramatically in the case of inhomogeneous field in Fig. 4(b), which disturbs the HHG trajectories and generates both odd- and even-order harmonic spectra. For the second HHG plateau, the spatial inhomogeneity dramatically affects the harmonic emission process, which presents enhancement processes around -0.25 o.c. and 0.75 o.c. and shows a suppressed process at 0.25 o.c. In order to further explain the phenomenon that only the second HHG plateau has a magnitude enhancement of two to three orders in the case of inhomogeneous field, we present the time-frequency analysis of the interband contributions in Figs. 4(c) and 4(d). It clearly shows a two- to three-order magnitude enhancement of the second HHG plateau, while the magnitude of the first HHG plateau is still comparable. This agrees with our analysis [13] that interband transitions play key roles in HHG and thus may explain why only the second plateau is dramatically enhanced.

We finally show energy band structure and time-dependent electron population of the conduction bands in Fig. 5. In

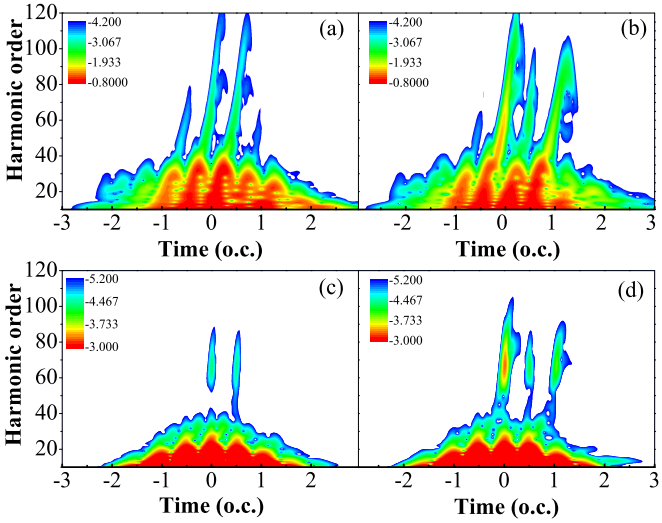

FIG. 4. Time-frequency analysis of HHG. Time-frequency analysis of HHG in a homogeneous field in panels (a) and (c) and an inhomogeneous field in panels (b) and (d). Panels (a) and (b) are time-frequency analyses with full contribution. Because the two HHG plateaus are mainly determined by interband contribution, we show time-frequency analysis of interband contribution in homogeneous field in panel (c) and inhomogeneous field in panel (d). The color is plotted on the logarithmic scale.

Figs. 5(a) and 5(b), one can find that the energy bands calculated by Bloch states agree well with those by the B-spline basis. The minimal gap between the valence band and the first conduction band is about 4.2 eV, which corresponds to harmonic order 11 in Fig. 2(b). According to the energy band structure and the population of the conduction bands, one can further get insight into the HHG enhancement. As previously mentioned, the harmonic plateaus are determined

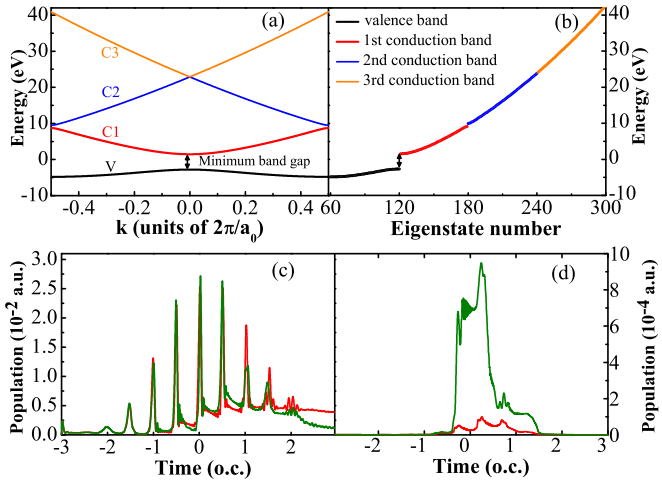

FIG. 5. Energy band structures and populations of conduction bands. Band structures calculated by Bloch states expansion are compared with the result obtained by the B-spline basis in panels (a) and (b), respectively. The electron populations as a function of time for the C1 band and C2 plus C3 band in homogeneous field (red curve) are illustrated in panels (c) and (d), respectively. The olive curves present results in the inhomogeneous field.

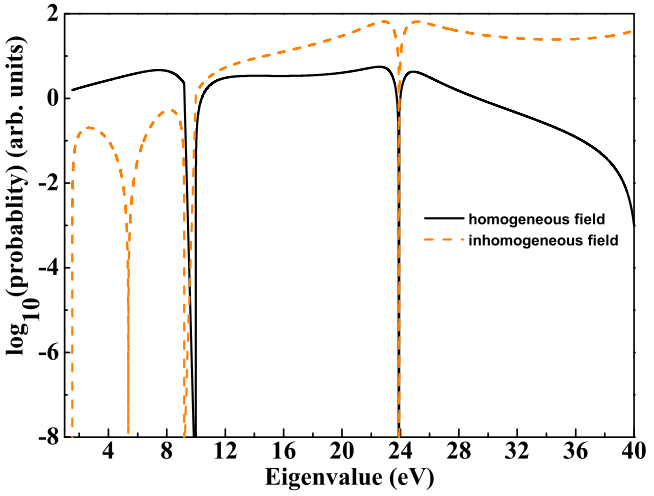

FIG. 6. Transitional probabilities of conduction bands. Transitional probabilities calculated by $|\langle\phi_{n_0}|\hat{x}|\phi_n\rangle|^2$ (black solid curve) for homogeneous field and an additional term $|\langle\phi_{n_0}|x^2|\phi_n\rangle|^2$ (orange dashed curve) for spatial inhomogeneous field.

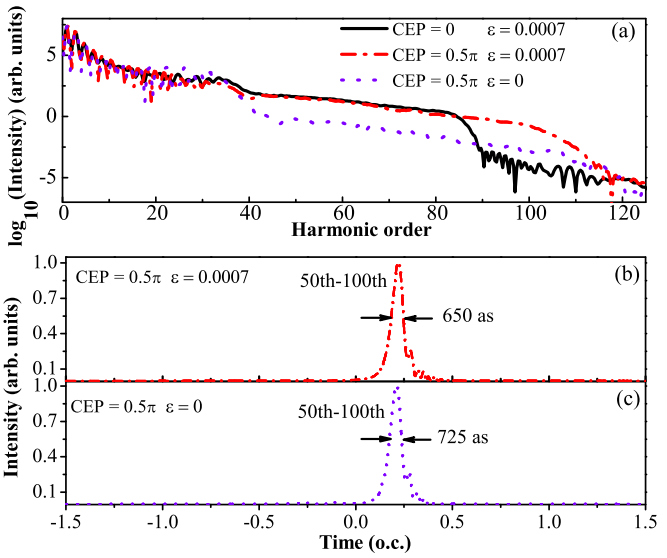

FIG. 7. Synthesis of attosecond pulses. (a) HHG in few-cycle laser fields. The inhomogeneity (ϵ) of laser fields is 0.0007. We choose two different CEP values, 0 and 0.5π. The violet dotted curve in panel (a) shows the HHG in the case of homogeneous field with CEP = 0.5π. The field parameters are the same as those in Fig. 2 except for the pulse duration. Attosecond pulses generated by synthesis of harmonics with order 50–100 in the case of the inhomogeneous field with $\epsilon = 0.0007$, CEP = 0.5π and in the case of the homogeneous field with CEP = 0.5π are presented in panels (b) and (c), respectively. The intensity has been normalized.

by the transition process between the conduction bands and valence band, i.e., interband contribution. Transition between the first conduction band and valence band contributes to the first plateau, while the second plateau is attributed to transitions between high-lying conduction bands and the valence band. In Fig. 5(c), it illustrates that the first conduction band electron population has a small increment in the case of the inhomogeneous field compared with that in the case of the homogeneous field, which explains why the change of the intensity of the first plateau is not obvious. However, in Fig. 5(d), one can clearly see that electron population of the second conduction band has a dramatic increment at the center of the laser pulse, which could lead to more electrons coupling to the valence band and give rise to two to three orders of enhancement of the second HHG plateau.

In addition, we calculate the transition probabilities between the conduction and the valence bands in Fig. 6, to reveal the population enhancement in the case of inhomogeneous fields. The effect of spatial inhomogeneity on the transition probabilities can be described by the additional term $|\langle\phi_{n_0}|x^2|\phi_n\rangle|^2$, in which n_0 represents the initial valence band state and n represents the conduction band states. One can clearly see two minimal values of transition probabilities in the case of homogeneous field (black solid curve) at the energy about 10 and 24 eV, which correspond to the two energy gap positions within the conduction bands in Figs. 5(a) and 5(b). The enhancement of transition probability is negligible in the first conduction band (corresponds to the energy range below 10 eV), while a one to two orders of enhancement of transition probability has been obtained in the conduction bands C2 and C3 (corresponds to the energy range from 10 to 40 eV) caused by the effect of spatial inhomoneity. This provides a deeper insight to the fact that one can just observe obvious enhancement of intensity in the second HHG plateau.

Due to the intensity enhancement of the second HHG plateau in the case of inhomogeneous field, it can be used for intense isolated attosecond pulse generation. In order to obtain a supercontinuous HHG spectra, we adopt three-cycle-duration pulses with inhomogeneity parameter $\epsilon = 0.0007$. In Fig. 7(a), one can also observe two to three orders of enhancement of intensity at the second HHG plateau in few-cycle pulses. The carrier-envelope phase (CEP) can be used to control the cutoff energy of HHG under the inhomogeneous fields. In Figs. 7(b) and 7(c), the coherent superposition of harmonics has been adopted in the case of inhomogeneous field with $\epsilon = 0.0007$ and homogeneous field with CEP = 0.5π. Isolated attosecond pulses with durations of 650 and 725 as are produced by superposing the harmonics with order 50–100. One can draw a conclusion that the spatially inhomogeneous fields cannot only realize two to three orders of enhancement of the second plateau but also control the HHG trajectories and narrow the width of the attosecond pulses.

In summary, by numerically solving the time-dependent Schrödinger equation, the HHG process in the solid-state materials under the action of a spatially inhomogeneous laser field is simulated in the coordinate space. The spatially inhomogeneous field has been demonstrated to be capable of realizing the dynamic control of quantum pathes. The two-band model is inadequate in this case. Multiband transitions and nonadiabatic effects have to be considered. Unlike the gas phase, the inhomogeneous fields changed the transition rules to the higher conduction bands in solids. As a result, a two to three order intensity enhancement of the second plateau can be obtained in the case of the inhomogeneous field, which is comparable with the intensity of the first plateau. The bigger transition probabilities to the high-lying conduction bands come from the enhancement of the transition matrix

elements. An efficient scheme to break the bottleneck of low damage threshold has been proposed. In the homogeneous laser field, the intensity of the second plateau is quite low. Only the intense first plateau in HHG is experimentally observed. This work sheds light upon enhancement of the second HHG plateau and a promising way to triple the range of HHG spectra in experimental measurements. This can also be used to generate intense narrow isolated attosecond pulses from solids.

The authors thank Mu-Zi Li and Xin-Qiang Wang very much for helpful discussions. This work is supported by the National Natural Science Foundation of China (Grants No. 11404376, No. 11561121002, and No. 11465016).

[1] P. B. Corkum, Phys. Rev. Lett. **71**, 1994 (1993).
[2] K. A. Pronin, A. D. Bandrauk, and A. A. Ovchinnikov, Phys. Rev. B **50**, 3473(R) (1994).
[3] K. A. Pronin and A. D. Bandrauk, Phys. Rev. Lett. **97**, 020602 (2006).
[4] J. Itatani *et al.*, Nature (London) **432**, 867 (2004).
[5] X. B. Bian and A. D. Bandrauk, Phys. Rev. Lett. **113**, 193901 (2014).
[6] O. Smirnova *et al.*, Nature (London) **460**, 972 (2009).
[7] S. Ghimire, A. D. DiChiara, E. Sistrunk, P. Agostini, L. F. DiMauro, and D. A. Reis, Nat. Phys. **7**, 138 (2011).
[8] O. Schubert, M. Hohenleutner, F. Langer, B. Urbanek, C. Lange, U. Huttner, D. Golde, T. Meier, M. Kira, S. W. Koch, and R. Huber, Nat. Photon. **8**, 119 (2014).
[9] T. T. Luu, M. Garg, S. Yu. Kruchinin, A. Moulet, M. Th. Hassan, and E. Goulielmakis, Nature (London) **521**, 498 (2015).
[10] G. Ndabashimiye, S. Ghimire, M. Wu, D. A. Browne, K. J. Schafer, M. B. Gaarde, and D. A. Reis, Nature (London) **534**, 520 (2016).
[11] G. Vampa, T. J. Hammond, N. Thiré, B. E. Schmidt, F. Légaré, C. R. McDonald, T. Brabec, D. D. Klug, and P. B. Corkum, Phys. Rev. Lett. **115**, 193603 (2015).
[12] M. Wu, S. Ghimire, D. A. Reis, K. J. Schafer, and M. B. Gaarde, Phys. Rev. A **91**, 043839 (2015).
[13] Z. Guan, X. X. Zhou, and X. B. Bian, Phys. Rev. A **93**, 033852 (2016).
[14] S. Kim, J. Jin, Y. J. Kim, I. Y. Park, Y. Kim, and S. W. Kim, Nature (London) **453**, 757 (2008).
[15] M. Sivis, M. Duwe, B. Abel, and C. Ropers, Nature (London) **485**, E1 (2012).
[16] T. Shaaran, M. F. Ciappina, and M. Lewenstein, Phys. Rev. A **87**, 053415 (2013).
[17] T. Shaaran, M. F. Ciappina, R. Guichard, J. A. Pérez-Hernández, L. Roso, M. Arnold, T. Siegel, A. Zaïr, and M. Lewenstein, Phys. Rev. A **87**, 041402(R) (2013).
[18] T. Shaaran, M. F. Ciappina, and M. Lewenstein, Phys. Rev. A **86**, 023408 (2012).
[19] M. F. Ciappina, T. Shaaran, and M. Lewenstein, Ann. Phys. **525**, 97 (2013).
[20] M. F. Ciappina, S. S. Acimovic, T. Shaaran, J. Biegert, R. Quidant, and M. Lewenstein, Opt. Express **20**, 26261 (2012).
[21] I. Yavuz, E. A. Bleda, Z. Altun, and T. Topcu, Phys. Rev. A **85**, 013416 (2012).
[22] L. X. He, Z. Wang, Y. Li, Q. B. Zhang, P. F. Lan, and P. X. Lu, Phys. Rev. A **88**, 053404 (2013).
[23] X. Cao, S. C. Jiang, C. Yu, Y. H. Wang, L. H. Bai, and R. F. Lu, Opt. Express **22**, 26153 (2014).
[24] I. Y. Park, S. Kim, J. Choi, D. H. Lee, Y. J. Kim, M. F. Kling, M. I. Stockman, and S. W. Kim, Nat. Photon. **5**, 677 (2011).
[25] A. Husakou, S. J. Im, and J. Herrmann, Phys. Rev. A **83**, 043839 (2011).
[26] J. A. Pérez-Hernández, M. F. Ciappina, M. Lewenstein, L. Roso, and A. Zaïr, Phys. Rev. Lett. **110**, 053001 (2013).
[27] J. Wang, G. Chen, S. Y. Li, D. J. Ding, J. G. Chen, F. M. Guo, and Y. J. Yang, Phys. Rev. A **92**, 033848 (2015).
[28] J. C. Slater, Phys. Rev. **87**, 807 (1952).
[29] P. G. Hawkins, M. Y. Ivanov, and V. S. Yakovlev, Phys. Rev. A **91**, 013405 (2015).
[30] N. E. Christensen and I. Gorczyca, Phys. Rev. B **50**, 4397 (1994).
[31] F. Litimein, B. Bouhafs, Z. Dridi, and P. Ruterana, New J. Phys. **4**, 64 (2002).
[32] S. Chelkowski, A. D. Bandrauk, and P. B. Corkum, Phys. Rev. A **92**, 051401 (2015).
[33] S. Chelkowski, A. D. Bandrauk, and P. B. Corkum, Phys. Rev. Lett. **113**, 263005 (2014).
[34] H. Bachau, E. Cormier, P. Decleva, J. E. Hansen, and F. Martín, Rep. Prog. Phys. **64**, 1815 (2001).
[35] M. D. Feit, J. A. Fleck Jr., and A. Steiger, J. Comput. Phys. **47**, 412 (1982).
[36] W. H. Xiong, J. W. Geng, J. Y. Tang, L. Y. Peng, and Q. Gong, Phys. Rev. Lett. **112**, 233001 (2014).
[37] C. Chandre, S. Wiggins, and T. Uzer, Physica D (Amsterdam, Neth.) **181**, 171 (2003).